Article

Effect of Water Content Variation on the Tensile Characteristic of Clayey Loess in Ili Valley, China

Penglin Zheng [1], Jinge Wang [1], Zihao Wu [1], Wei Huang [2], Changdong Li [1] and Qingbing Liu [1,*]

[1] Badong National Observation and Research Station of Geohazards (BNORSG), China University of Geosciences (Wuhan), 388 Lumo Road, Wuhan 430074, China
[2] The Seventh Geological Brigade of Hubei Geological Bureau, 111 Lanxin Road, Yubei, Chongqing 400042, China
* Correspondence: qingbing@cug.edu.cn

Abstract: The mechanical behavior of loess is highly predicated on variation in its moisture content. While the impacts of the water content on the shearing behavior and collapsibility of loess have been extensively studied, its effect on tensile characteristics has received relatively little attention. In this study, a series of tensile tests were conducted on remolded specimens of a clayey loess that were collected from Ili Valley in China. Two sets of loess specimens with varying water contents were prepared separately using wetting and drying methods. The influence of the water content on the tensile stress–strain response, failure mode and tensile strength was investigated by combining the tensile test results and particle image velocimetry (PIV) analysis. On this basis, a nuclear magnetic resonance (NMR) test and scanning electron microscopy (SEM) observations were implemented in order to assist with the interpretation of the underlying mechanism. The test results indicate that the tensile failure process and the variation of tensile strength with varying water contents differ for specimens that are prepared with wetting and drying methods; a finding which arises from the differences in the soil microstructure, clay–water interaction and the distribution of capillary and adsorbed water. This research has shown that the tensile strength of clayey loess is essentially dominated by the clay's hydration/cementation and the development of capillary and adsorption suction as well as the microstructural evolution that occurs with the change in the water content. Based on the experimental observations, a conceptual model is proposed in order to interpret the effect of water content on loess' tensile behavior.

Keywords: clayey loess; tensile strength; tensile failure; water content; microstructure; capillary water; adsorptive water

1. Introduction

Loess deposits are widely distributed in northwest China and they cover an area of about 640,000 km^2, roughly equivalent to 6.7% of China's total land area [1,2]. Geohazards as well as failures in earth constructions frequently occur in these regions due to the local geomorphic features coupled with the special characteristics of loess, leading to non-negligible losses of human lives and properties [3–6]. Loess is water sensitive; the deterioration of its mechanical properties due to water infiltration is acknowledged to contribute greatly to the occurrences of many geo-hazards and this has been extensively studied, with attention having largely been paid to the loess' collapsibility and shear strength behavior [7–9]. Despite this, the role that is played by the loess' tensile characteristics has been increasingly recognized. For example, the weak tensile strength of loess was noted to be a primary reason for ground fissures [6] and, furthermore, a large amount of loess landsides present in the form of a cracking–sliding failure mode. This is a mode which is characterized by the development of tensile fractures on the crests of slopes followed by sliding movement [2,10]. Therefore, a clear understanding of the tensile behavior of loess is of practical significance.

The tensile strength of soil can be measured using direct methods (e.g., uniaxial and triaxial tensile tests) or indirect methods (e.g., a flexure beam test, double punch test, unconfined penetration test or Brazilian tensile test) [11–18]. The direct methods have advantages such as their ability to reveal a definite stress–strain relationship and their straightforward manner in determining tensile strength; however, difficulties in specimen clamping, misalignment, stress concentration and friction at the ends of the specimen could lead to considerable inaccuracy of the measurements [19,20]. The superiority of indirect methods lies in the simplicity of their specimen preparation and testing procedures; however, the tensile strength needs to be deduced based on stress distribution theory, highly relying on the assumed mechanical and boundary conditions. In the past decades, with the development of testing methodology and apparatus, the tensile behaviors of various types of soils were investigated [21–25]. As for loess, [6] showed that its tensile strength decreased with an increase in its water content and a decrease in its dry density. A similar observation was made by [26], which examined the tensile characteristics of Q_3 loess around Lanzhou city using an unconfined penetration test (UPT) and found that the tensile strengths that were derived from the UPT were lower than those that were measured in a direct tension test and that they were well correlated with the unconfined compressive strength. A comprehensive review of the studies of the tensile strength of Malan loess was presented by [2] and the results indicated the dependency of the tensile strength on the water content, dry density, test method, specimen size and loading rate. In addition, the tensile behavior of loess was perceived to be significantly affected by its texture and structure; for example, Sun et al. (2016) observed that the tension resistance of fractured loess was controlled by the orientation of the joints plane [27] while Wang et al. (2019) illustrated that a vibration-induced change in the microstructure of loess led to its tensile strength degradation [28]. While these existing studies have revealed the main factors influencing the tensile behavior of loess, the mechanism behind the evolution of the tensile characteristics with the change in water content, density and soil structure was rarely investigated and poorly understood.

The water content is no doubt among the most critical factors affecting loess' tensile characteristics [8,9]. Loess has long been considered as an unsaturated soil with an open and metastable structure, characterized by the skeleton granules (i.e., silt and sand particles) that are bonded to some extent by water-sensitive cementing agents such as clay minerals and carbonates [28–30]. The intactness of such a structure can be preserved by these cementations along with the capillary forces that originate from matric suction and surface tension; however, loess is very susceptible to fluctuation in its moisture content. In other words, the structure tends to alter as a consequence of the changes in cementation and suction that are induced by wetting/drying [31]. The tensile resistance of loess, in essence, originates from the bonding force between its soil particles which is provided by cementing agents as well as soil suction and, in this sense, the effect of the water content on the tensile property of loess is closely linked to the structure/fabric status, which involves the degree and pattern of the cementation, particle contact manner, pore structure, etc. [32]. This linkage, however, has not been well understood in view of the fact that the existing studies on this aspect mainly focus on the macroscopic level. Beyond this, previous studies have paid little attention to loess containing high amounts of clay particles. For this kind of loess, the clay cementations and hydration are supposed to play a dominant role in the magnitude of the bonding force between the particles and the development of soil suction. However, a comprehensive understanding of clay–water interaction and its effect on the tensile behavior of clayey loess at varying water contents is lacking.

The aim of the present work is, therefore, to look into the evolution of the tensile characteristics of clayey loess in response to water content variation and to explore the associated microscopic mechanism. To this end, direct tension tests were performed on a clayey loess using a newly developed tensile device with a particle image velocimetry (PIV) technique that was exploited in order to assist in analyzing the tensile displacement/strain field as well as the tensile cracking development. The microstructures of specimens with

varying water contents were characterized by the use of scanning electron microscopy (SEM) observations and the distribution of the pore water was identified using the nuclear magnetic resonance (NMR) approach. Through the combined use of all of these tests' results, a conceptual framework was finally presented for understanding the effect of water content on the tensile behavior of clayey loess. The novelty of this study lies in the following aspects: (1) it demonstrates that the variation in tensile strength with water content displays different tendencies between the specimens that were prepared according to the drying and wetting paths; (2) the relative roles of capillary water and adsorbed water in the development of the tensile resistance of clayey loess is, for the first time, clearly revealed; (3) a novel conceptual model illustrating the effects of clay hydration/cementation and the accompanied microstructural change on tensile behavior is proposed.

2. Test Apparatus

The apparatus that was used for the tensile tests is schematically shown in Figure 1; it is comprised of two parts: a direct tension testing system and an image capture system. As is illustrated in Figure 2, the tension testing system adopts an '8' shaped split mold, which is specially designed to reduce the central cross-sectional area of the soil specimen in order that the tensile fracture can occur at its middle part. Similar shapes of mold have been applied in [33,34] and they have been shown to enable the tensile failure to take place at the center neck section. During the test, the mold with the prepared soil specimen was placed upright on the platform where one half of the mold was clamped to the fixed end of the platform through an S-type load cell while the other half was connected to a movable frame that was driven by an electric motor to pull the specimen forward in the horizontal direction with a given displacement rate (ranging from 0.01 mm/min to 10 mm/min). A linear sliding roller was fabricated and placed between the mold and the base plate of the platform in order to minimize the mechanical friction. The S-type load cell that was screwed into the immovable half of the mold was employed in order to measure the tensile force and it had a range of 0–500 N with a 0.02% full scale (FS) accuracy. The tensile displacement was recorded by a LVDT (with a capacity of 20 mm and accuracy of 0.1%FS) that was attached to the movable half of the mold, as is indicated on Figure 2. Prior to the test, the connections between all of these components were carefully examined and adjusted so as to ensure their tightness. Therefore, it is reasonable to envisage that the specimen deformed synchronously with the loading and measuring devices.
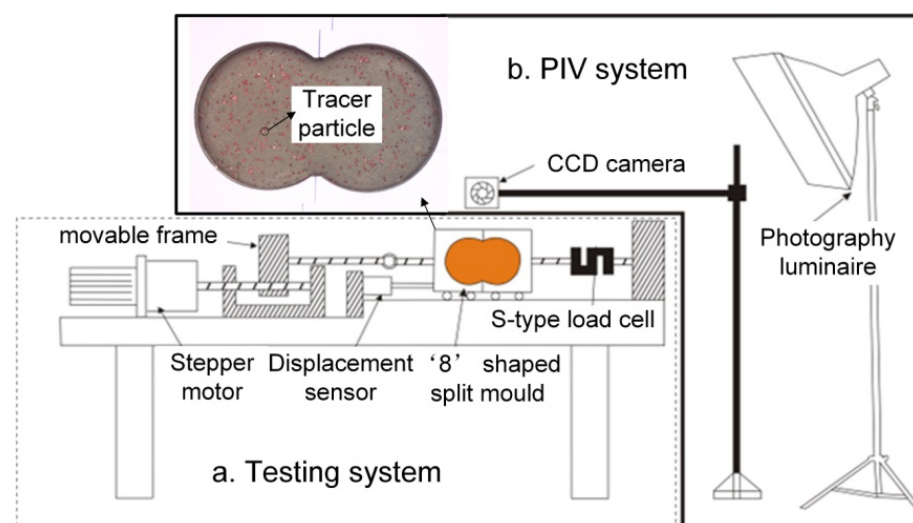

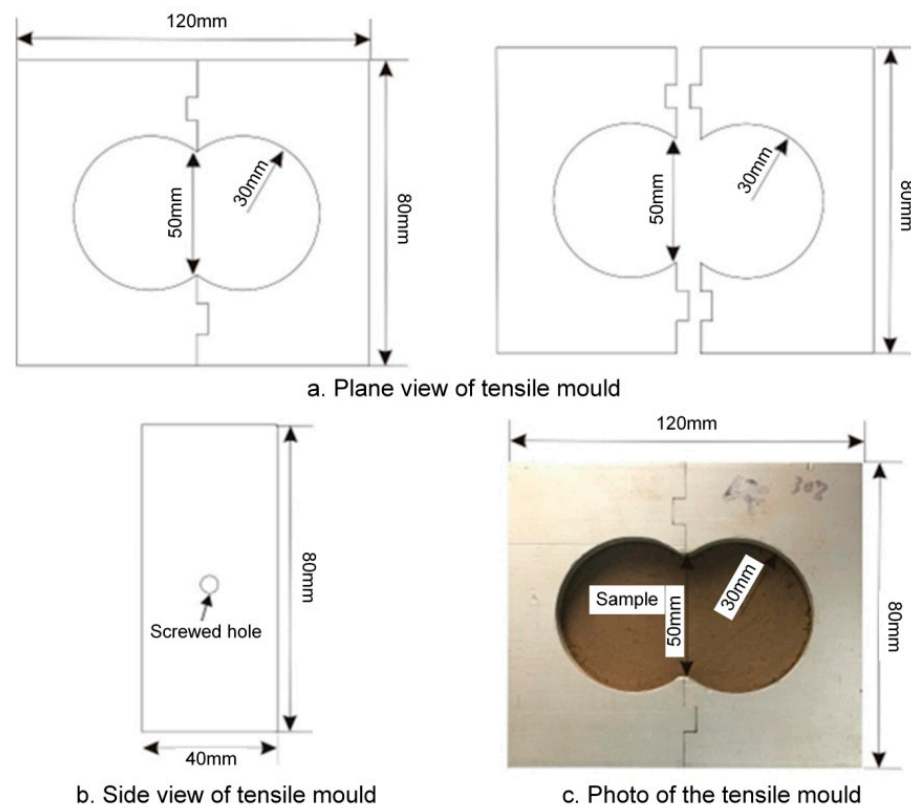**Figure 1.** The apparatus developed for tensile tests.

Figure 2. The '8' shaped split mold employed for tensile tests.

The image capture system involved a high-resolution (16.1 megapixel) camera that was placed right in front of the tested specimen and photographic luminaire equipment that was used to create even and diffused light in order to enhance the quality of the photography. The tensile deformation and failure process of the soil specimen was automatically recorded by the camera which was set to capture images at certain intervals. These images were then used for PIV analysis through the use of an open software named Geo-PIV so as to obtain the information regarding the tensile strain and displacement within the region of interest (ROI) on the specimen's surface.

3. Materials and Methods

3.1. Basic Indices of Ili Loess

The loess that was used in the presently described experiments was collected from the Mohuer River landslide in Ili Valley, Xinjiang and it is a kind of Malan loess (Q_3 loess). The sampling position was around the rear edge of the landslide where tensile cracks had developed and the sampling depth was approximately 0.5 m, as is indicated in Figure 3. The grain grading curve of the test loess is presented in Figure 4, which shows that it is composed of primarily silt-sized particles at a fraction of 74.9%, clay particles (21.5%) and sand particles (3.6%) and that it can be classified as clayey loess due to its relatively high clay content [35]. The basic indices of the Ili loess were measured in the laboratory and they are provided in Table 1; the loess contains a certain soluble salt content, with mass fractions of soluble salt (mainly Na_2SO_4) and slightly soluble salt ($CaSO_4$) of 1.52% and 0.15%, respectively. The mineral composition of the loess sample, which was determined using X-ray diffraction (XRD), is shown in Table 2.
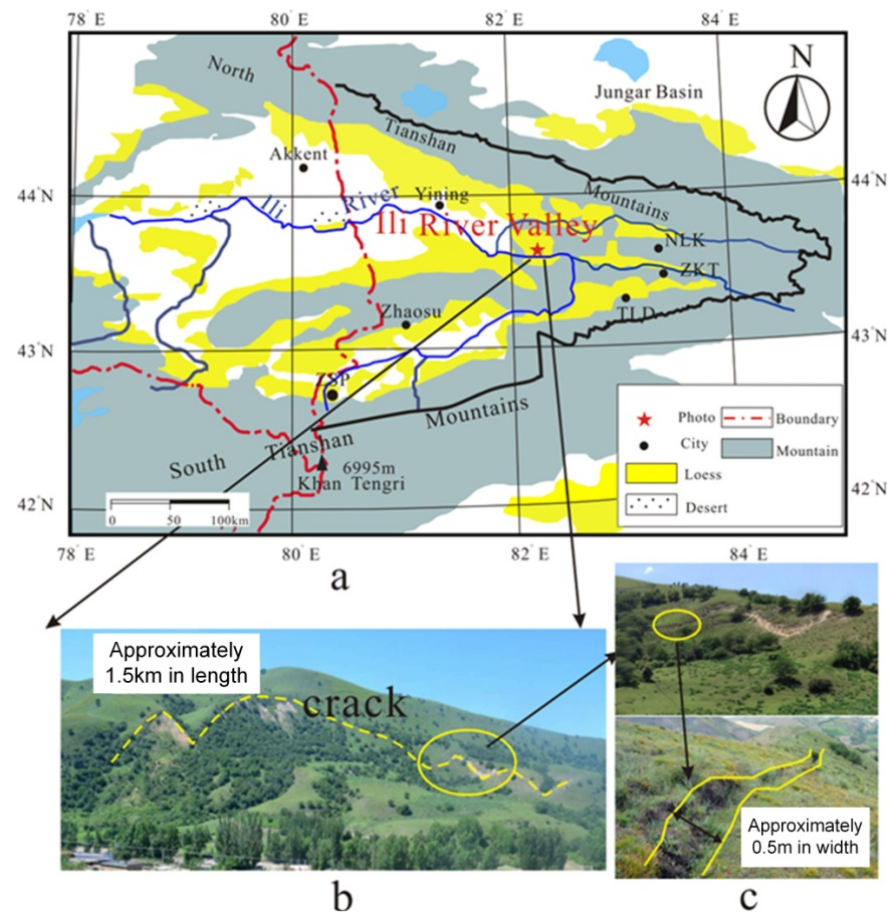
Figure 3. Tensile cracks on the crest of the loess landslide in Ili river valley: (**a**) distribution of loess deposits in Ili area (modified from Song et al. (2014), Figure 2 [36]); (**b,c**) the details of loess' tensile cracks.
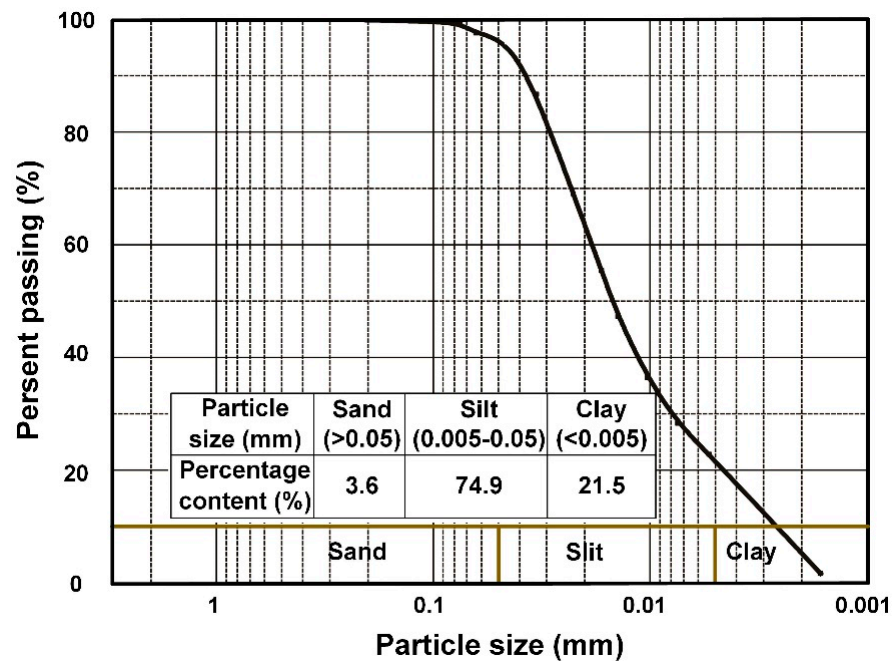

Figure 4. Grain grading curve of the investigated Ili loess.

Table 1. Basic properties of the Ili loess.

Specific Gravity G_S	Natural Water Content w_a (%)	Liquid Limit (%)	Plastic Limit (%)	Plasticity Index	Soluble Salt Na_2SO_4 (%)	Less Soluble Salt $CaSO_4$ (%)
2.64	14.1	28.2	19.1	9.15	1.52	0.15

Table 2. Mineral composition of the Ili loess.

Mineral	Quartz	Illite	Albite	Chlorite	Calcite
Content (%)	37.77	28.80	12.03	11.53	9.87

3.2. Tensile Test Procedure

The drying and wetting specimen preparation paths were considered separately for the purpose of examining the effect of water content variation on loess' tensile behavior. Accordingly, two methods were adopted in order to prepare the loess specimens for the tensile tests. The first method was to prepare a batch of specimens by gradually increasing their water contents and this is hereafter referred to as the wetting method (WM). The other method, termed the drying method (DM), involves firstly preparing several specimens with a water content that is close to the liquid limit and then air-dry them to different target water contents.

For the WM, the loess was dried in an oven at 105 °C, crushed and then sieved through a 2 mm sieve. Different amounts of distilled water were added to the sieved soil in order to achieve the target water contents (i.e., 6%, 10%, 14%, 18%, 22% and 26%). The wet soil was subsequently kept in a sealed container for 24 h so as to ensure water equalization. The tensile specimens were prepared with the mold that is shown in Figure 2 and they were compacted to three different dry densities (i.e., 1.4, 1.6 and 1.8 g/cm^3) using light compaction equipment. For the DM, the sieved soil was firstly moistened to a water content that was approximately equal to its liquid limit and then it was compacted within the tensile mold to the desired dry densities (i.e., 1.4, 1.6 and 1.8 g/cm^3). After that, the compacted specimens were carefully transferred to desiccators in order to reduce their water contents. The specimens were weighed at intervals until the target water contents were attained (i.e., 6%, 10%, 14%, 18%, 22% and 26%). Finally, all of the prepared specimens were subjected to the tensile test at a constant displacement rate of 0.1 mm/s along the horizontal direction.

As is illustrated in Figure 1, the tensile force (F) that was mobilized was measured by the load cell while the tensile displacement (S) was recorded by LVDT. The tensile stress (σ) and strain (ε) were determined using the following equation [37], wherein A is the cross-sectional area of the neck part of the specimen and equals 9.6 cm^2 and L (100 mm) is the total length of the specimen.

$$\sigma = F/A; \; \varepsilon = S/L \tag{1}$$

In the process of the tensile test, the tensile stress (σ) increased gradually until a peak value was achieved. This peak stress is defined as the tensile strength (σ_t) of the specimen and represents the maximum stress that the specimen can resist against before it succumbs to tensile failure [38]. Furthermore, parallel tests were conducted on three duplicated specimens for each dry density and water content in order to ensure the repeatability of the tests.

3.3. Particle Image Velocimetry Analysis (PIV)

The particle image velocimetry (PIV) technique was applied in order to analyze the displacement and strain field on the surface of the specimen that was subjected to each tensile test. The principle of the PIV method is to detect the movement of the trace (or

marker) particles in a sequence of images, identify the same particle in different images and generate deformation information by comparing tracing particles. For the implementation of this technique, a thin layer of red quartz sand with an average grain size of 0.5 mm was evenly sprinkled and lightly pressed onto the surface of the loess specimens. These sand particles served as trace particles for PIV analysis, as is illustrated in Figure 1. During the test, the specimen's surface was photographed at a time interval of 10 s with a high-resolution industrial camera. The captured photographs were imported into Geo-PIV software and the region of interest (ROI), including the neck part of the tensile specimen, was selected for analysis. The image correlation algorithm was invoked in order to obtain the displacement of the same tracer particle in any two consecutive images and, by comparing the subsequent images with the reference image (the one that was taken before the test), the deformation information within the ROI at the different tensile stages could be obtained and illustrated in the output images by displacement vectors and different colors representing the strain levels.

3.4. Nuclear Magnetic Resonance Test (NMR)

In recent years, nuclear magnetic resonance (NMR) has been widely used for the study of pore water within rock and soil because of its fast, effective, non-contact and non-destructive manner of measurement [39,40]. The basic principle of the NMR method is to apply a radio frequency magnetic field to a target in order to promote the energy transition of the nucleus (i.e., proton ^{1}H of soil water) and detect the relaxation processes after removing the applied magnetic field. The measured variation of the NMR signal (free induction decay) with time, referred as the FID curve, is correlated with the transverse relaxation time T_2, which is a measure of the mobility of the water molecule [41]. The T_2 distribution can be determined by the use of the Fourier inversion of the FID curve and it usually shows distinct peaks, a property which reflects the different energy states of the pore water. This method, therefore, can be used for distinguishing capillarity-dominated water from adsorption-dominated water. The amount of each type of water can be represented by the peak area (under the T_2 curve) within the corresponding T_2 regime [42]. In this study, all of the loess specimens that were prepared with the aforementioned wetting and drying methods were subjected to NMR tests; the relative amounts of capillary and adsorbed water in each specimen were derived based on the T_2 measurements so as to assist in analyzing the mechanism of the loess' tensile strength's variation with its water content.

3.5. Scanning Electron Microscope Test (SEM)

Prior to the tensile tests, a series of microstructural observations were made on the loess specimens with varying water contents using a Hitachi SU3500 scanning electron microscope. The specimens were cut into small clods with the dimensions of 2 cm × 2 cm × 2 cm and then freeze-dried in order to preserve the soil structure. After that, the clods were carefully broken off by hand and the selected fresh surface was subjected to gold coating using sputtering equipment and then subsequently taped to an aluminum mounting disk for SEM observations. The aim of SEM observation is to aid the interpretation of the tensile characteristics from the perspective of microstructural changes. Figure 5 presents a flow chart illustrating the methodology that was followed in this study.
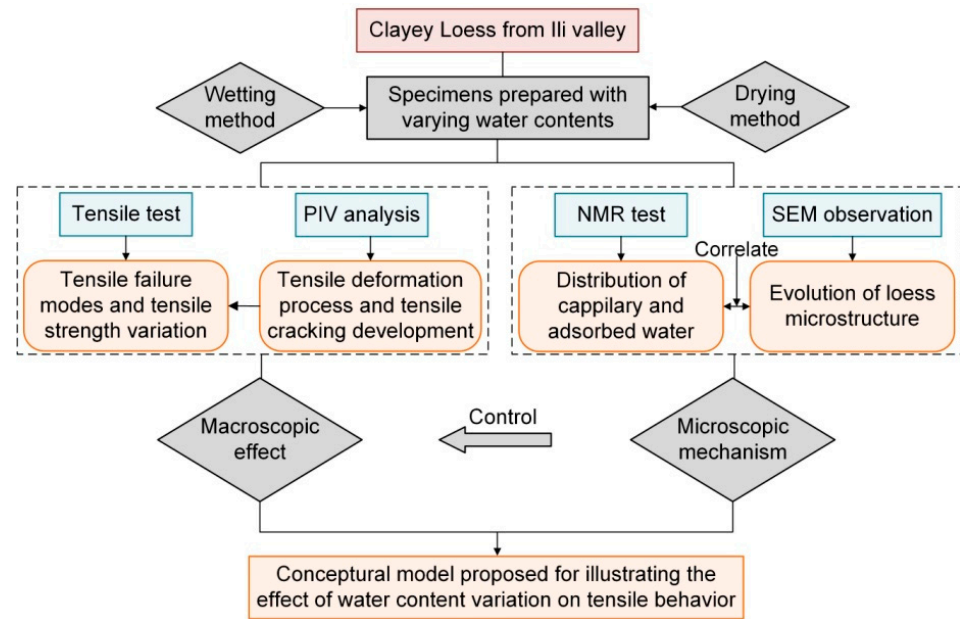
Figure 5. The methodology employed in this study.

4. Results

4.1. Tensile Failure Mode

The tensile stress–strain curves for the specimens with a dry density of 1.6 g/cm^3 are shown in Figure 6, where ε and σ refer to the tensile strain and tensile stress, respectively.
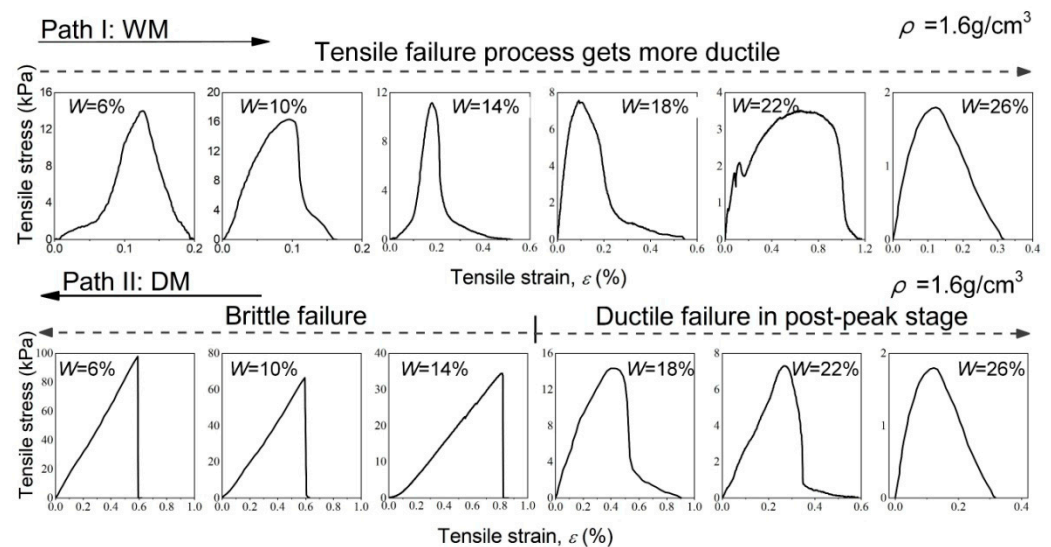

Figure 6. Tensile stress–strain curves for specimens with different water contents (ρ = 1.6 g/cm^3).

For the specimens that were prepared using the WM (i.e., along the wetting path), their tensile stress–strain curves were found to have a similar pattern. It was shown that the tensile stress increased gradually until a peak stress value was reached and then the stain-softening behavior appeared at the post-peak stage. The analogously plastic deformation after reaching the peak tensile stress indicates the ductile behavior of all of the specimens that were prepared using the wetting method. Their tensile failures can be described approximately as ductile failures. It was noted that the ductile failure was more evident as the water content increased.

Unlike the WM samples, the tensile stress–strain responses for the specimens that were prepared using the DM present two distinct patterns: (1) when the water content was more than 18%, the tensile failure was, in general, ductile, similar to that of the WM

samples; (2) when the water content was less than 18%, the tensile stress initially increased almost linearly with the tensile strain until the peak value was reached. Then, the tensile stress decreased abruptly to 0 kPa with no plastic strains following afterward, apparently indicating a brittle failure mode.

The tensile deformation process of loess is accompanied by the evolution of the strain field and the development of tensile cracks; two traits that are well captured by using PIV analysis. Combined with the obtained PIV results, the tensile stress–strain curve that is related to the ductile failure mode can be divided into four stages: the fabric adjustment stage (I), micro-crack formation stage (II), macro-crack formation stage (III) and crack penetration stage (IV), as are indicated in Figure 7. The PIV analysis results from the central neck part of the soil specimen for these four stages are illustrated in Figure 8, wherein Part A shows the development of the surface cracks while Parts B and C present the distribution of the displacement vector and strain contours at the region of interest (ROI). It was seen that, in stage I, the difference between the tensile displacement vectors, along with a relatively greater tensile strain, appeared at the upper part of the ROI, implying that the soil fabric was being adjusted due to the external tensile force and that the forthcoming tensile crack may develop from the upper part. In stage II, the tensile stress gradually increased to its peak value and micro-cracks were expectedly formed at the upper part of the specimen. The strain contour plot shows that the larger strain was mainly concentrated within the region wherein the micro-cracks emerged and that the tensile strain was at its largest near the crack's tip. In this stage, the local structure of the specimen was destroyed. In stage III, macro-cracks gradually formed, leading to a rapid decrease in the tensile stress. There was a noticeable displacement difference between the two sides of the crack and the direction of displacement was nearly perpendicular to the crack. Furthermore, a relatively greater tensile strain occurred at the bottom of the ROI, indicating the potential propagation of the crack from the upper part of the sample to the bottom. After the specimen entered stage IV, the crack extended downward and the tensile stress gradually decreased to zero. The larger tensile strain that appeared at the bottom of the sample indicated the formation of the connected crack. At this stage, the tensile displacement on the left side of the crack was close to zero, implying the splitting of the specimen and the occurrence of complete tensile failure.
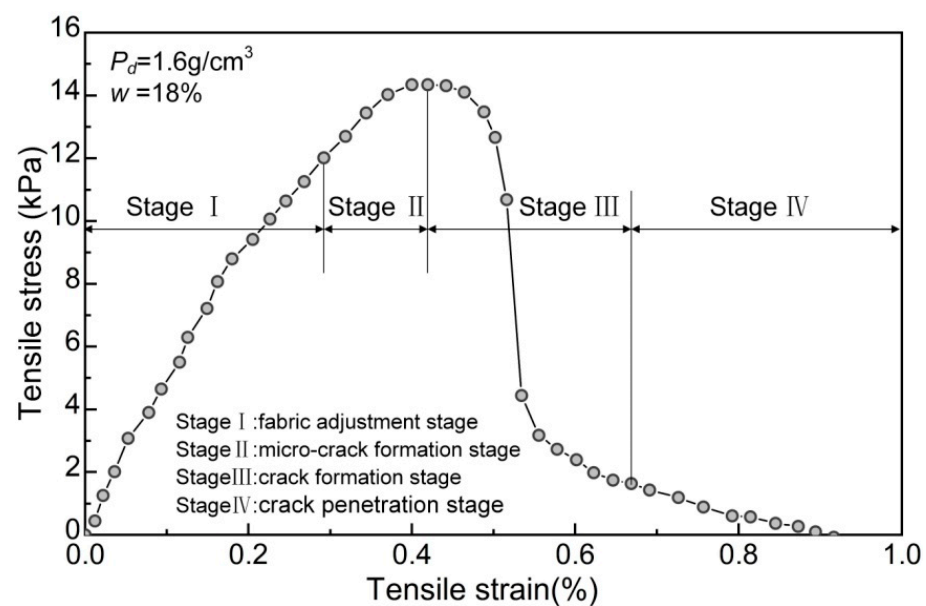

Figure 7. The typical tensile stress–strain curve for the ductile failure mode.
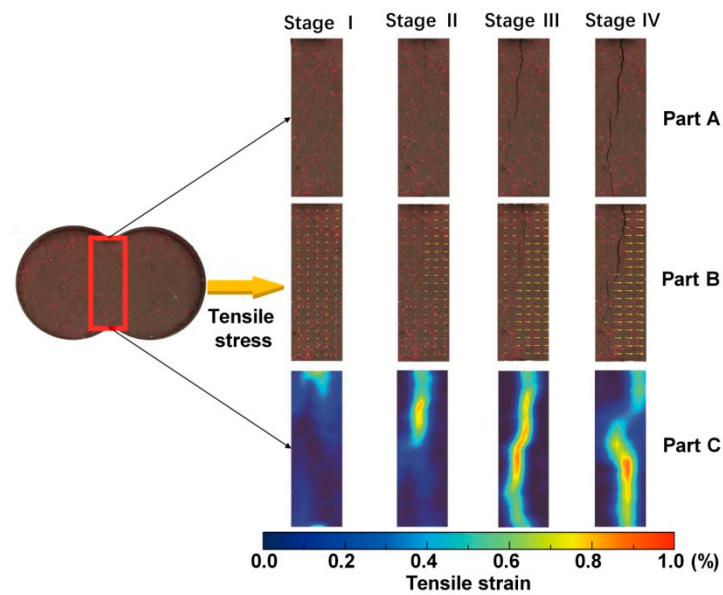
Figure 8. Tension deformation process obtained from PIV analysis.

Similarly, the overall tensile stress–strain curve for the brittle failure mode can be segmented into two stages: the fabric adjustment stage (I) and the crack penetration stage (II), as are illustrated in Figure 9. In stage I, no cracks were observed and the tensile stiffness of the sample remained almost constant during the process of the soil structure's adjustment, as was indicated by the linear increase in the tensile stress with the strain. When the peak tensile stress was attained, the curve entered stage II. In this stage, the tensile cracks developed and penetrated throughout the sample very rapidly, leading to a sharp decrease in the tensile stress to zero and remarkable fracture brittleness. As this stage lasted for a very short time, no photos of the post-peak failure process were captured and used for the PIV analysis.
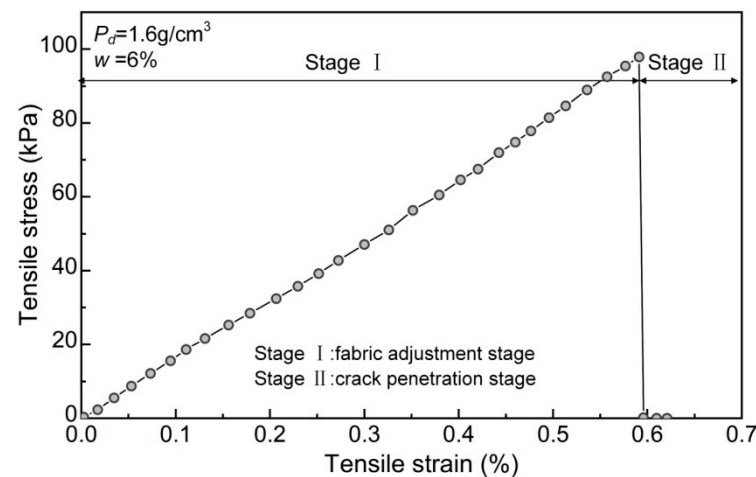

Figure 9. The typical tensile stress–strain curve for the brittle failure mode.

4.2. Tensile Strength

The experimental results show that the peak strength of all of the remolded loess specimens varied from 1.31 to 115 kPa and demonstrate that the tensile strength of remodeled loess was significantly influenced by its water content and dry density (Figure 10). For the same water content and dry density, the tensile strength of the DM specimen was consistently greater than that of the WM specimen, with the strength difference between the two groups becoming more profound as the water content decreased, as is indicated in Figure 10.
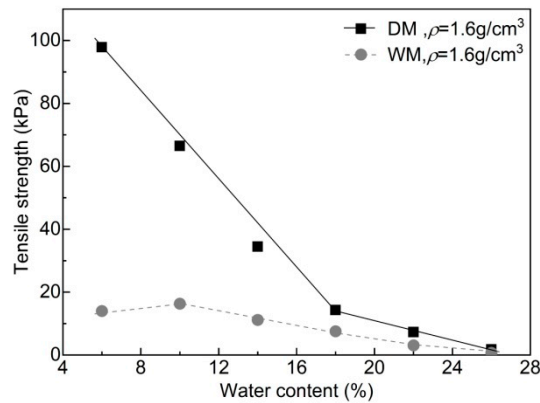
Figure 10. The overall trend for the tensile strength to vary with water content (ρ = 1.6 g/cm^3).

The variations of the tensile strength with the water content for the DM and WM samples with different dry densities are presented in Figure 11. In terms of the DM specimens, the tensile strength generally increased as the water content decreased and it can be seen from Figure 11a that there exists a critical water content (w_c) of about 18% which divides the overall variation curve into two different regimes. It was noted that the w_c value is close to the plastic limit of the loess. When the water content was greater than w_c, the tensile strength increased very slowly with the decrease in the water content; when the water content was less than w_c, the tensile strength increased very rapidly (at a higher rate of increase) as the water content decreased. These observations imply that the proximity of the water content to the plastic limit leads to a substantial change in the factors contributing to loess' tensile strength. The variation with the water content of the tensile strength of the WM specimens, however, showed a dissimilar tendency. As is demonstrated in Figure 11b, the tensile strength initially increased as the water content increased to 10% and it then decreased quickly with the further increases in the water content. A boundary water content of 10% that separates the two different trends can be identified and the tensile strength achieved its peak value at this water content. It is commonly believed that an increase in the water content leads to a decrease in soil suction and, hence, the cohesive forces between soil particles, which induces the reduction of soil's tensile strength. However, Figure 11b indicates that this common understanding seems not to be applicable to the WM specimens with relatively low water contents (<10%). The water distribution status in loess and the associated microstructure evolution with water content change should be considered to be an important reason accounting for the tendency that is shown in Figure 11b, which will be discussed later.
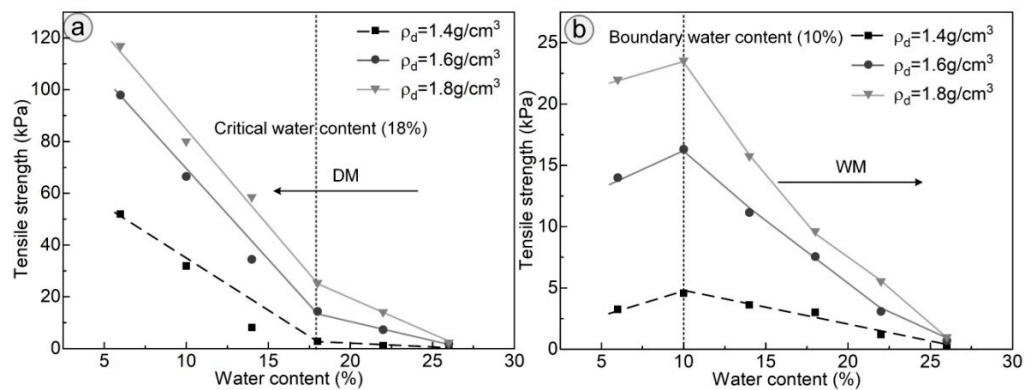

Figure 11. The variation of tensile strength with water content for (**a**) DM specimens and (**b**) WM specimens.

Figure 11 also indicates that, for a given water content, the tensile strength, overall, increased with the increase in the dry density. Moreover, the role of the dry density varied

with the range of the water content. For the DM sample, the rate of increase in the tensile strength with the decreased water content increased with the dry density in samples with a water content of between 18% and 26%. When the water content was less than <18%, the slope of the tensile strength curve increased as the dry density increased from 1.4 g/cm^3 to 1.6 g/cm^3 and then it remained almost unchanged with a further increase in the dry density to 1.8 g/cm^3, as is illustrated in Figure 11a. With respect to the WM sample, the slope of the tensile strength versus the water content curve is not affected by the dry density at a water content of less than 10% (Figure 11b); when the water content was higher than 10%, the rate of decrease in the tensile strength with increased water content increased with the dry density.

4.3. Variation of Microstructure with Water Content

Figure 12 shows representative SEM images of the DM and WM specimens with dry densities of 1.6 g/cm^3 at varying water contents. Figure 12a–c presents the evolution of the microstructure of the loess along the drying path (i.e., the DM). It can be seen that, at high water content of 26%, the clay particles were fully hydrated and dispersedly attached onto the surface of the skeleton particles of the loess (i.e., silt, sand or their aggregates) in the form of 'floc' (see the red circle). Obviously, the cementation between the skeleton particles that was provided by the dispersed clay was rather weak; besides this, the particles were in contact with each other in a point–point manner with bracket and 'mosaic' pores developed between them (shown by the white rectangle). Such a microstructural configuration led to a lower capacity of the sample to resist external tension. With the decrease in the water content to 18%, the clay started the aggregation process and connected the skeleton particles in the form of clay bridges and clay 'buttresses', as is illustrated by the red circle in Figure 12b. Part of inter-particle pores were filled with aggregated clay–silt clusters (see the white rectangle). Under this condition, the degree of clay cementation together with the cohesion between the particles enhanced leading to the improvement of the tensile strength. When the water content was further reduced to 6%, the clay's cementation significantly increased, which firmly bonded the particles, and the prevalence of inter-particle pores decreased. As is indicated in Figure 12c, the overall soil fabric was stable with the boundaries between the individual particles becoming unclear. Such a stable microstructure contributes to the high tensile strength of the DM specimens with low water contents.

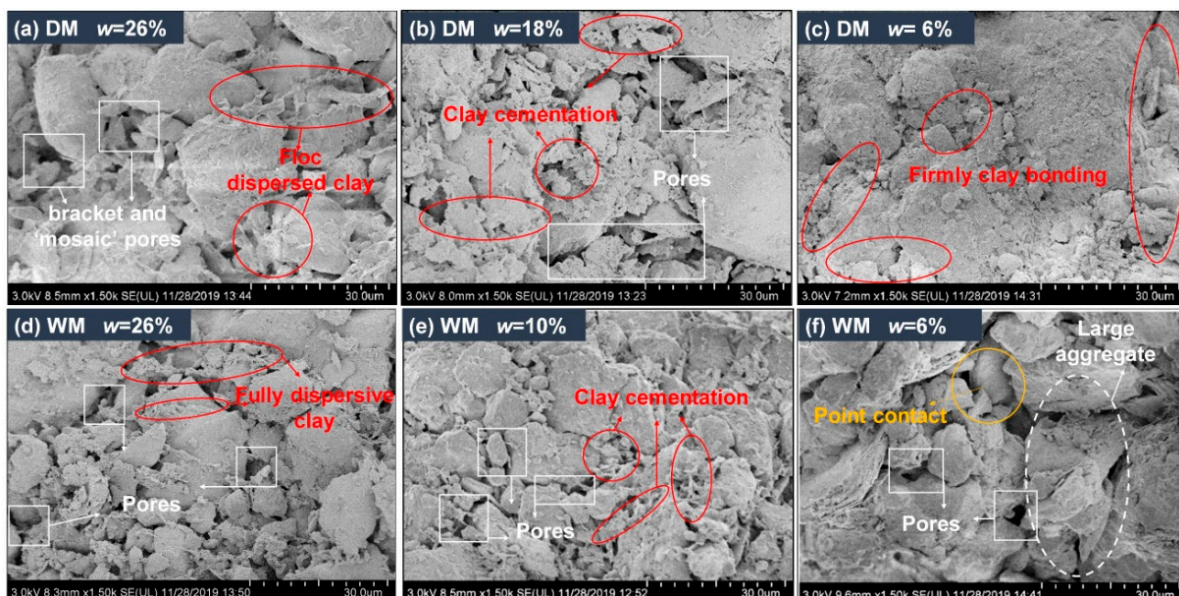
Figure 12. SEM images of Ili loess with different water contents for (**a**) DM-w = 26% specimen (**b**) DM-w = 18 specimen (**c**) DM-w = 6 specimen (**d**) WM-w = 26 specimen (**e**) WM-w = 10 specimen (**f**) WM-w = 6 specimen.

The microstructures of the WM specimens are shown in Figure 12d–f. It is obvious that the WM and DM specimens with the same water contents have different microstructural characteristics. For example, the structure of the WM specimen with a water content of 6% is dominated by the point–point contact of the silt particles and large aggregates; these large aggregates are the assembly of clay, silt and sand particles. There is little clay cementation presented at the contact area of the silt aggregates (Figure 12f). These observations are distinct from those that are shown in Figure 12c. The reason for this distinction originates from the two different sample preparation methods. The weak connection between the silt and aggregates of the WM specimens at low water contents led to their low tensile resistance. When the loess was wetted to a higher water content of 10%, the hydration of the clay compositions disassembled the large aggregates into small ones, with the hydrated clay connecting adjacent silts and smaller aggregates, as is indicated in Figure 12e. The enhancement of the clay bonding rendered the improvement of the cohesive force of the soil particles and, hence, the increase in the tensile strength. With a further increase in the water content to 26%, the clay particles were fully dispersive (Figure 12d), causing the clay's cementation between the skeleton particles to vanish. The soil pores were filled with free water, resulting in very weak cohesive force and low tensile strength.

4.4. Identification of Water Distribution

The distribution of the pore water and related soil–water interactions varied during the drying and wetting processes of the loess, processes which are closely related to the evolution of the loess' tensile strength. Therefore, it is necessary to identify the soil water distribution of loess specimens in order to shed light on the effect of their water content. As aforementioned, the relaxation time (T_2) measurement in the NMR test reflects the mobility of the water molecules and it can be employed for distinguishing capillary water and adsorbed water as they are retained by the soil through different forces. Figure 13 depicts the example T_2 distribution curves for loess specimens with a dry density of 1.6 g/cm^3 that were prepared along the drying path. There are two distinct peaks in the curve which represent the different energy states of the pore water. The left peak with a shorter relaxation time T_2 is related to the adsorbed water in the soil pores whereas the right peak with a longer relaxation time T_2 is associated with capillary (free) water.
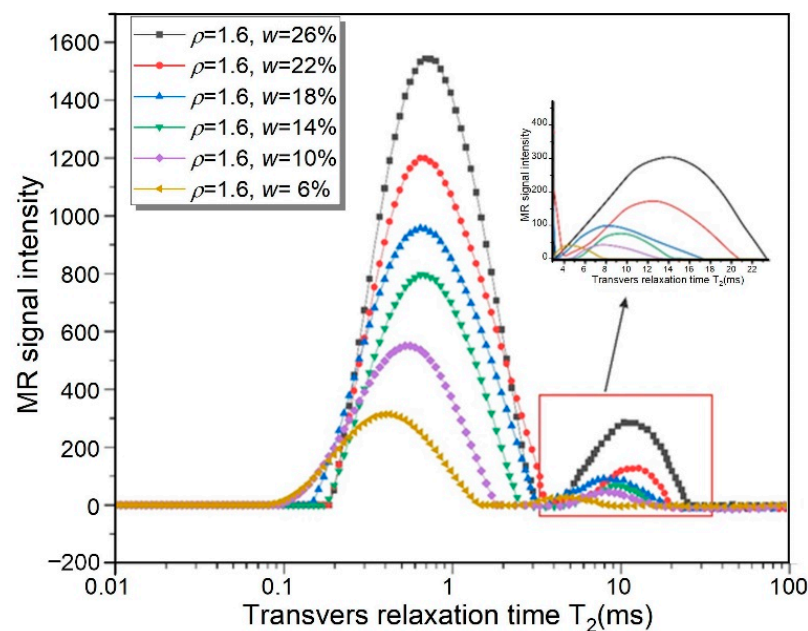

Figure 13. T2 distribution curves for DM specimens.

The peak area, defined as the area under the T_2 distribution curve, represents the amount of pore water [37]. As such, the relative contents of capillary and adsorbed water can be determined by their respective peak areas. The calculated capillary and adsorbed water contents for the loess specimens along both the drying and wetting paths (i.e., the DM and WM) are shown in Figure 14. It can be seen that, for the DM specimens, the decrease in the water content from 26% to 18% led to a great reduction of the capillary water amount and an insignificant decrease in the amount of adsorbed water; when $w < 18\%$, the further drying of the loess sample was primarily contributed to by the loss of adsorbed water, with only a very slight change in the capillary water fraction. It is interesting to find that the demarcation water content (18%) for the variation of the two forms of pore water agrees well with the critical water content (w_c) where the tensile strength shifts from the slow- to the fast-increase stage (as is illustrated in Figure 11a), indicating that the transition of loess' tensile strength is closely related to the difference in the solid–water interaction between capillarity-dominated and adsorption-dominated stages. As for the WM specimens, the initial increase in the water content to 10% led to a rapid increase in the adsorbed water amount and little variation in the amount of capillary water, as is indicated in Figure 14. Thereafter, the amount of capillary water increased at a higher rate than the adsorbed water as the specimen was further moisturized. It is worth noting that the peak tensile strength that was achieved at the water content of 10% for the DM specimen (see Figure 11b) seems to be linked to the initially rapid increase in the adsorbed water.
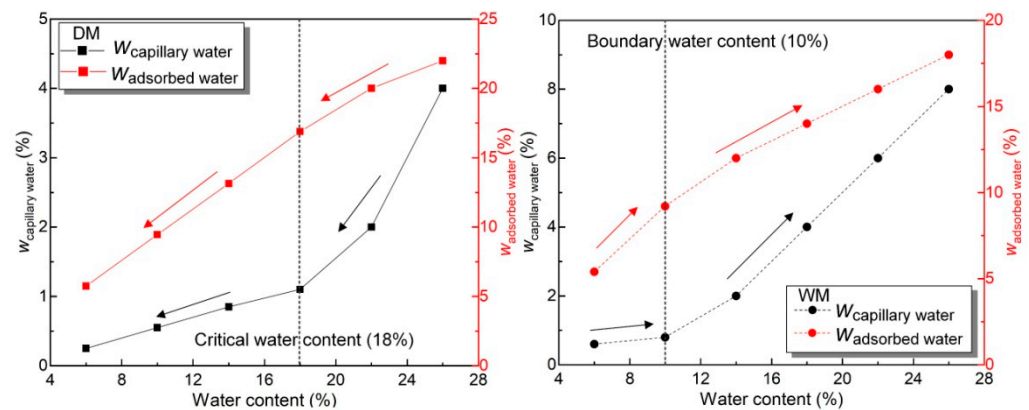

Figure 14. Capillary and adsorbed water contents within DM and WM specimens for the arrow in DM represents the drying direction and the arrow in WM represents the wetting direction.

5. Discussion

The above test results highlight that the influence of the water content on loess' tensile behavior significantly differs between specimens that were prepared according to the wetting and drying paths and that it is associated with the distribution of pore water and the evolution of the soil structure as well as the soil–water interaction mechanism. Generally, the tensile strength of loess derives from the cohesion of its soil particles [43], which is related to four kinds of physical and physiochemical origins: (1) clay bonding arising from the short-range clay–water interaction [28,29,31]; (2) capillary attraction due to the existence of a water bridge or capillary meniscus between soil particles [13,44]; (3) soluble and less soluble bonding agents [45] and (4) carbonate cementations (an origin which is only considered for intact loess) [46]. By considering these four mechanisms and combining the results of the tensile test, microstructural observation and NMR analysis, a conceptual model for interpreting the tensile strength variation of loess with its water content is proposed and illustrated in Figure 15.
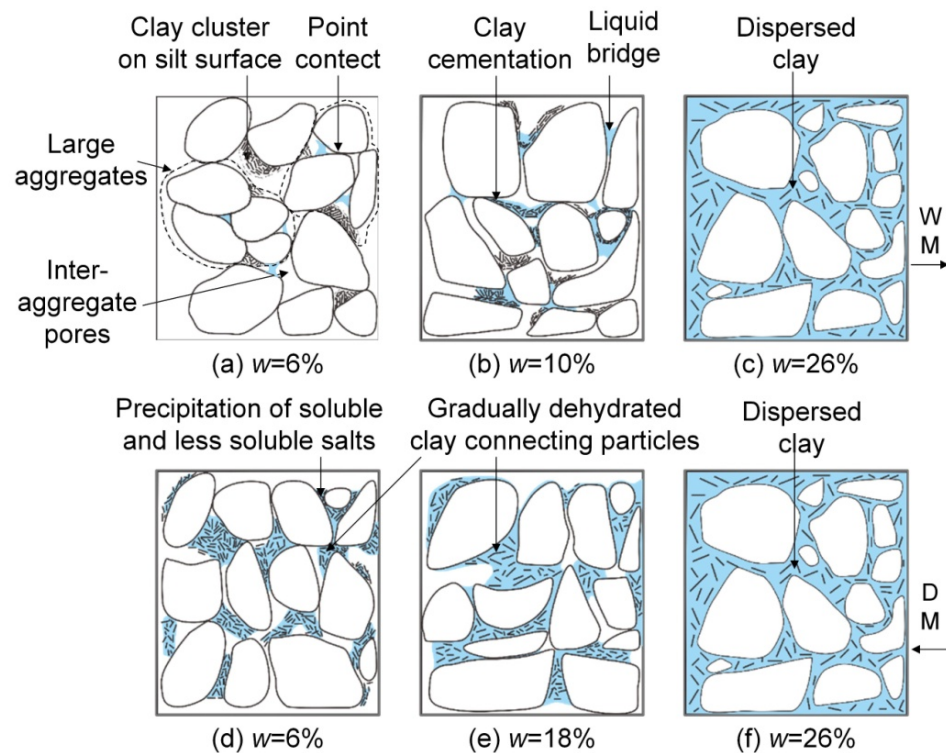
Figure 15. A conceptual model for interpreting the evolution of tensile behavior of loess for (**a**) WM-*w* = 6% specimen (**b**) WM-*w* = 10 specimen (**c**) WM-*w* = 26 specimen (**d**) DM-*w* = 6 specimen (**e**) DM-*w* = 18 specimen (**f**) DM-*w* = 26 specimen.

A remolded loess specimen that has been compacted with a low water content usually possesses an aggregated structure as it is prepared by reconstructing the crushed soil powder of intact loess [47]; part of the intact structure is preserved and presented in the form of the large aggregate particles which are assemblies of clay, silt and sand that are created through clay and carbonate cementation, as is shown in Figure 15a. Water mainly exists inside of the aggregates, with little water bridging or connecting the aggregates. In this case, the mechanical behavior of a loess specimen with a low water content is more like that of granular soil and it exhibits very low tension resistance. As more water is added to the loess, the water gradually surrounds the surfaces of the aggregates, with liquid bridges forming between the aggregates. The liquid bridges at the contact points act as bonding agents that effectively improve the cohesion of the aggregates (see Figure 15b). Furthermore, the hydration of the clay commences, which provides additional cementation between the skeleton particles (e.g., silt–silt or silt–aggregate). All of these factors contribute to the increase in the loess' tensile strength [44]. When the water content reaches a certain value (i.e., 10%), the liquid bridge is fully developed and the clay cementation is enhanced to its maximum; at this point the peak tensile strength is attained. This explains the reason for the observed increase in the tensile strength of the WM specimens with the increase in the water content to 10%. When the loess is compacted with a relatively high water content, the dissolution of soluble salt and clay hydration leads to the formation of a dispersed structure, which is characterized by the individual silt and sand particles or small-sized aggregates being surrounded by fully dispersive clay platelets. The connection that is provided by a liquid bridge or clay cementation is lost. Furthermore, the soil suction and capillary attraction forces decrease with the increase in the saturation degree [32]. Therefore, the tensile strength reduces and shows a decreasing trend with the increase in the water content, as is illustrated by the Figure 11b at *w* > 10%.

Unlike the specimens that were prepared with the wetting method, the DM specimens were prepared by air-drying the previously compacted specimens of high water content

to different target water contents. The evolution of the soil structure and the solid–liquid interaction are both different in this scenario. When the water content decreased from 26% to 18%, the NMR test indicated the predominant loss of the capillary water amount. At a higher water content, the cohesive force of the soil particles primarily arises from the capillary attraction which increases with a decrease in the capillary water content [48]. Furthermore, the dispersive clay platelets become aggregated at the contact points of the skeleton particles as the water content reduces, which adds to the overall cementation effect (Figure 15e). Therefore, the tensile strength gradually increases at this stage. With the further drying of the specimens, the water that is present in the loess is mainly from the decreasing amount of adsorbed water that is firmly attached to the clay particles, as is indicated in Figure 14. The dehydration of the clay significantly enhances the clay's cementation and induces a quick increase in the soil suction due to the short-range clay–water interaction. It can be noted that the developed soil suction within the adsorption-dominated regime is generally several orders of magnitude higher than that which is within the capillarity-dominated regime [48]. Therefore, the tensile strength increased at a higher rate when $w < 18\%$, which explains the two distinct stages of tensile strength variation that are shown in Figure 11a. Moreover, the energy dispersive X-ray analysis that was performed on the specimens with water contents of 6% revealed that the Ca and Na elements were detected at the contact points between the particles (Figure 16), indicating the precipitation of soluble and less soluble salts at very low water content. Obviously, the recovery of soluble and less soluble bonding agents at low water contents contributes to the further improvement of the resistance of loess to tensile failure. Furthermore, the transition from brittle failure to ductile failure of the DM specimens at the critical water content of 18% (Figure 6) is ascribed to the fact that the consistency of the loess changes at the onset of the adsorbed water-dominated stage.
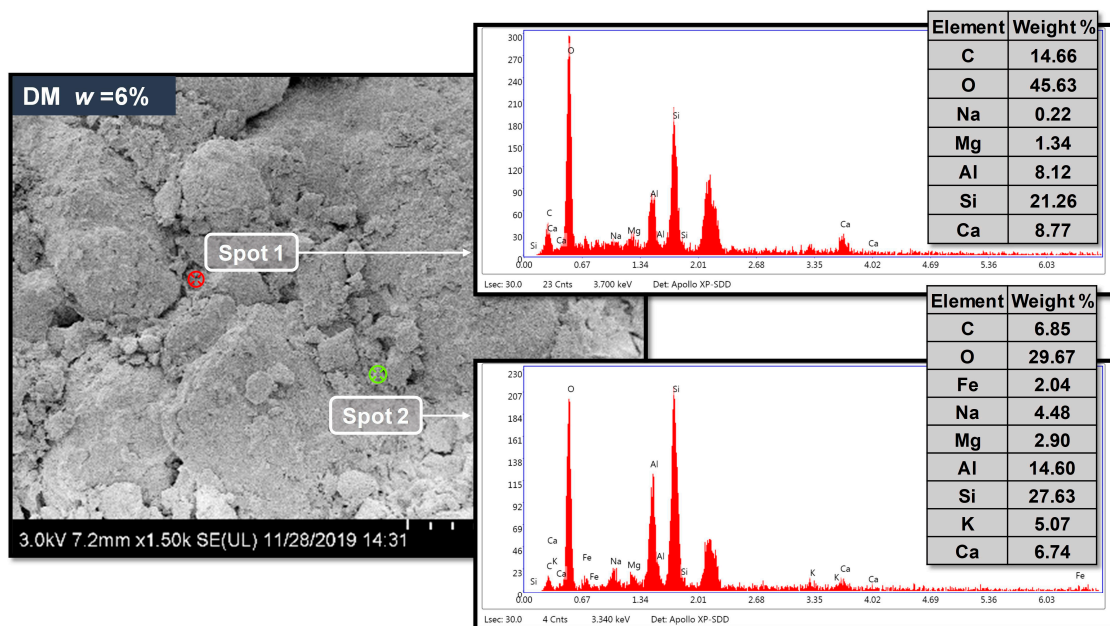

Figure 16. Energy dispersive spectrometer (EDS) analysis of the DM specimen at $w = 6\%$.

　　It is worth mentioning that the studied loess is a clayey loess containing a clay faction as high as 21.5%, thus the clay cementation, clay–water interaction and adsorbed water content play important roles in analyzing the effect of the water content on the loess' tensile behavior. As for loess with diminished clay composition, such as sandy loess, capillary effects are a dominating factor affecting the tensile behavior over the unsaturated water content range, in addition to the inherent salt and carbonate cementations.

6. Conclusions

In this study, the effect of water content on the tensile behavior of a clayey loess was investigated by conducting a series of tensile tests on remolded loess specimens with varying water contents that were prepared with two different methods (the DM and WM). PIV, SEM and NMR analysis were performed in order to assist with the interpretation of the underlying mechanism. The following conclusions can be drawn.

(1) The tensile characteristics of the DM and WM specimens are different. The WM specimens, in general, had lower tensile strength than the DM specimens and the former presented a ductile tensile failure mode while the failure process for the latter shifted from brittleness to ductility as the water content increased. The PIV results revealed the correlation between the tensile stress–strain response, the distribution of strain field and the development of tensile cracks.

(2) The tensile strength of the WM specimen initially increased with the water content and then decreased with a further increase in the water content, whereas the tensile strength of the DM specimens increased with the decrease in water content at two distinct rates. SEM observation and NMR tests indicated that the different trends for the tensile strength to vary according to the water content derived from the differences in the soil microstructure and the relative amount of capillary and adsorbed water, as well as the interaction between the clay and water.

(3) The effect of the water content's variation on the tensile strength of a remolded clayey loess is essentially linked to the evolutions of the clay's hydration/cementation, the development of capillary and adsorption suction and the accompanied microstructure change. This complicated linkage can be depicted using the proposed conceptual model that is presented in Figure 15.

Author Contributions: Experimental design: P.Z., J.W. and Q.L.; Tensile experiment: P.Z. and W.H.; SEM and NMR test: Z.W., J.W. and W.H.; Experimental analysis: P.Z., Z.W. and C.L.; Data analysis: P.Z., W.H. and C.L.; Writing—original draft preparation: P.Z.; Funding acquisition: Q.L. and C.L. All authors have read and agreed to the published version of the manuscript.

Institutional Review Board Statement: Not applicable.

Data Availability Statement: Not applicable.

Conflicts of Interest: The authors declare no conflict of interest.

References

1. Peng, D.; Xu, Q.; Qi, X.; Fan, X.; Dong, X.U.; Li, S.; Ju, Y. Study on Early Recognition of Loess Landslides Based on Field Investigation. *Int. J. Geohazards Environ.* **2016**, *2*, 35–52. [CrossRef]
2. Li, Y. A review of shear and tensile strengths of the Malan Loess in China. *Eng. Geol.* **2018**, *236*, 4–10. [CrossRef]
3. Zhuang, J.; Peng, J.; Wang, G.; Iqbal, J.; Wang, Y.; Li, W.; Xu, Q.; Zhu, X. Prediction of rainfall-induced shallow landslides in the Loess Plateau, Yan'an, China, using the TRIGRS model. *Earth Surf. Proc. Land.* **2017**, *42*, 915–927. [CrossRef]
4. Juang, C.H.; Dijkstra, T.; Wasowski, J.; Meng, X. Loess geohazards research in China: Advances and challenges for mega engineering projects. *Eng. Geol.* **2019**, *251*, 1–10. [CrossRef]
5. Peng, J.; Sun, P.; Igwe, O.; Li, X.A. Loess caves, a special kind of geo-hazard on loess plateau, northwestern China. *Eng. Geol.* **2018**, *236*, 79–88. [CrossRef]
6. Sun, P.; Peng, J.; Chen, L.; Yin, Y.; Wu, S. Weak tensile characteristics of loess in China—An important reason for ground fissures. *Eng. Geol.* **2009**, *108*, 153–159. [CrossRef]
7. Wen, B.; Yan, Y. Influence of structure on shear characteristics of the unsaturated loess in Lanzhou, China. *Eng. Geol.* **2014**, *168*, 46–58. [CrossRef]
8. Li, P.; Vanapalli, S.; Li, T. Review of collapse triggering mechanism of collapsible soils due to wetting. *J. Rock Mech. Geotech. Eng.* **2016**, *8*, 256–274. [CrossRef]
9. Wu, L.Z.; Zhou, Y.; Sun, P.; Shi, J.S.; Liu, G.G.; Bai, L.Y. Laboratory characterization of rainfall-induced loess slope failure. *Catena* **2017**, *150*, 1–8. [CrossRef]

10. Zhang, P.; Xiao, P.; Yao, W.; Liu, G.; Sun, W. Profile distribution of soil moisture response to precipitation on the Pisha sandstone hillslopes of China. *Sci. Rep.* **2020**, *10*, 9136. [CrossRef]

11. Ghosh, A.; Subbarao, C. Tensile Strength Bearing Ratio and Slake Durability of Class F Fly Ash Stabilized with Lime and Gypsum. *J. Mater. Civil Eng.* **2006**, *18*, 18–27. [CrossRef]

12. Kim, T.H.; Kim, C.K.; Jung, S.J.; Lee, J.H. Tensile strength characteristics of contaminated and compacted sand-bentonite mixtures. *Environ. Geol.* **2007**, *52*, 653–661. [CrossRef]

13. Lu, N.; Wu, B.; Tan, C.P. Tensile strength characteristics of unsaturated sands. *J. Geotech. Geoenviron.* **2007**, *133*, 144–154. [CrossRef]

14. David Suits, L.; Sheahan, T.C.; Nahlawi, H.; Chakrabarti, S.; Kodikara, J. A Direct Tensile Strength Testing Method for Unsaturated Geomaterials. *Geotech. Test. J.* **2004**, *27*, 11767. [CrossRef]

15. Narvaez, B.; Aubertin, M.; Saleh-Mbemba, F. Determination of the tensile strength of unsaturated tailings using bending tests. *Can. Geotech. J.* **2015**, *52*, 1874–1885. [CrossRef]

16. Stirling, R.A.; Hughes, P.; Davie, C.T.; Glendinning, S. Tensile behaviour of unsaturated compacted clay soils—A direct assessment method. *Appl. Clay Sci.* **2015**, *112–113*, 123–133. [CrossRef]

17. Pincus, H.J.; Dass, R.N.; Yen, S.C. Tensile Stress-Strain Characteristics of Lightly Cemented Sand. *Geotech. Test. J.* **1994**, *17*, 305–314. [CrossRef]

18. Li, X.; Liu, Y.; Jiang, L.; Tang, Y. Determination of Tensile Strength of Compacted Loess by Double Punch Test. *Adv. Mater. Res.* **2011**, *194–196*, 1176–1179. [CrossRef]

19. Ge, L.; Hwang, Y.W.; Sun, H.M.; He, G.D.; Chen, R.P.; Kang, X. Effective Tensile Strength of Lightly Cemented Sand. *J. Mater. Civil Eng.* **2019**, *31*, 04018350. [CrossRef]

20. Kim, T.; Kim, T.; Kang, G.; Ge, L. Factors Influencing Crack-Induced Tensile Strength of Compacted Soil. *J. Mater. Civil Eng.* **2012**, *24*, 315–320. [CrossRef]

21. Divya, P.V.; Viswanadham, B.V.S.; Gourc, J.P. Evaluation of Tensile Strength-Strain Characteristics of Fiber-Reinforced Soil through Laboratory Tests. *J. Mater. Civil Eng.* **2014**, *26*, 14–23. [CrossRef]

22. Ibarra, S.Y.; Mckyes, E.; Broughton, R.S. Measurement of tensile strength of unsaturated sandy loam soil. *Soil Tillage Res.* **2005**, *81*, 15–23. [CrossRef]

23. Varsei, M.; Miller, G.A.; Hassanikhah, A. Novel Approach to Measuring Tensile Strength of Compacted Clayey Soil during Desiccation. *Int. J. Geomech.* **2016**, *16*, D4016011. [CrossRef]

24. Zhang, B.Y.; Li, Q.M.; Yuan, H.N.; Sun, X. Tensile Fracture Characteristics of Compacted Soils under Uniaxial Tension. *J. Mater. Civil Eng.* **2015**, *27*, 04014274. [CrossRef]

25. Sun, W.Y.; Liang, Q.G.; Yan, S.H.; Er-Feng, O.U.; Shao, S.L. Experimental study on tensile strength of undisturbed Q2 loess from Yan'an, Shanxi, China. *J. Geomech.* **2022**, *21*, 386–392.

26. Liang, Q.; Wu, X.; Li, C.; Wang, L. Mechanical analysis using the unconfined penetration test on the tensile strength of Q3 loess around Lanzhou City, China. *Eng. Geol.* **2014**, *183*, 324–329. [CrossRef]

27. Sun, P.; Peng, J.; Chen, L.; Lu, Q.; Igwe, O. An experimental study of the mechanical characteristics of fractured loess in western China. *B. Eng. Geol. Environ.* **2016**, *75*, 1639–1647. [CrossRef]

28. Wang, J.; Li, P.; Gu, Q.; Xu, Y.; Gu, T. Changes in tensile strength and microstructure of loess due to vibration. *J. Asian Earth Sci.* **2019**, *169*, 298–307. [CrossRef]

29. Assadi-Langroudi, A.; Ng'Ambi, S.; Smalley, I. Loess as a collapsible soil: Some basic particle packing aspects. *Quatern. Int.* **2018**, *469*, 20–29. [CrossRef]

30. Assallay, A.M. *Structure and Hydrocollapse Behaviour of Loess*; Loughborough University of Technology: Loughborough, UK, 1998.

31. Zhou, B.; Wu, Y.; Chan, J.; Wang, S.; Qiao, Z.; Hu, S. Wetting-drying cycles enhance the release and transport of autochthonous colloidal particles in Chinese loess. *Hum. Ecol. Risk Assess.* **2019**, *25*, 335–353. [CrossRef]

32. Li, H.; Tang, C.; Cheng, Q.; Li, S.; Gong, X.; Shi, B. Tensile strength of clayey soil and the strain analysis based on image processing techniques. *Eng. Geol.* **2019**, *253*, 137–148. [CrossRef]

33. Vesga, L.F.; Vallejo, L.E. Direct and Indirect Tensile Tests for Measuring the Equivalent Effective Stress in a Kaolinite Clay. In Proceedings of the Fourth International Conference on Unsaturated Soils, Carefree, AZ, USA, 2–6 April 2006; pp. 1290–1301.

34. Tamrakar, S.B.; Toyosawa, Y.; Mitach, T.; Itoh, K. Tensile strength of compacted and saturated soils using newly developed tensile strength measuring apparatus. *Soils Found.* **2005**, *45*, 103–110. [CrossRef]

35. Liu, T.S. *Loess and the Environment*; Science Press: Beijing, China, 1985.

36. Song, Y.; Chen, X.; Qian, L.; Li, C.; Li, Y.; Li, X.; Chang, H.; An, Z. Distribution and composition of loess sediments in the Ili Basin, Central Asia. *Quatern. Int.* **2014**, *334–335*, 61–73. [CrossRef]

37. Young, W.C. *Roark's Formulas for Stress and Strain*; McGraw-Hill: New York, NY, USA, 2003.

38. Bai, Y. Fatigue Crack Monitoring of T-Type Joints in Steel Offshore Oil and Gas Jacket Platform. *Sensors* **2021**, *21*, 3294.

39. Tan, L.; Wei, C.; Tian, J.; Zhou, H. Experimental study of unfrozen water content of frozen soils by low-field nuclear magnetic resonance. *Rock Soil Mech.* **2015**, *36*, 1566–1572.

40. Jäger, A.; Schaumann, G.E.; Bertmer, M. Optimized NMR spectroscopic strategy to characterize water dynamics in soil samples. *Org. Geochem.* **2011**, *42*, 917–925. [CrossRef]

41. Tian, H.H.; Wei, C.F.; Lai, Y.M.; Chen, P. Quantification of Water Content during Freeze Thaw Cycles: A Nuclear Magnetic Resonance Based Method. *Vadose Zone J.* **2018**, *17*, 1–12. [CrossRef]

42. Gao, S.; Chapman, W.G.; House, W. Application of low field NMR T2 measurements to clathrate hydrates. *J. Magn. Reson.* **2009**, *197*, 208–212. [CrossRef]

43. Lambe, T.; Whitman, R. *Soil Mechanics*; Wiley: New York, NY, USA, 1979.

44. Tang, C.S.; Pei, X.J.; Wang, D.Y.; Shi, B.; Li, J. Tensile Strength of Compacted Clayey Soil. *J. Geotech. Geoenvironmental Eng.* **2015**, *141*, 04014122. [CrossRef]

45. Li, Y.; Zhao, J.; Li, B. *Loess and Loess Geohazards in China*; CRC Press/Balkema: Boca Raton, FL, USA, 2017.

46. Wuddivira, M.N.; Camps-Roach, G. Effects of organic matter and calcium on soil structural stability. *Eur. J. Soil Sci.* **2007**, *58*, 722–727. [CrossRef]

47. Romero, E. A microstructural insight into compacted clayey soils and their hydraulic properties. *Eng. Geol.* **2013**, *165*, 3–19. [CrossRef]

48. Lu, N. Generalized Soil Water Retention Equation for Adsorption and Capillarity. *J. Geotech. Geoenvironmental* **2016**, *142*, 04016051. [CrossRef]